

Hyper-Eddington mass accretion onto a black hole with super-Eddington luminosity

Yuya Sakurai^{1*}, Kohei Inayoshi², Zoltán Haiman²

¹*Department of Physics, School of Science, University of Tokyo, Bunkyo, Tokyo 113-0033, Japan*

²*Department of Astronomy, Columbia University, 550 W. 120th Street, New York, NY 10027, USA*

Draft version 7 July 2016

ABSTRACT

We perform one-dimensional radiation hydrodynamical simulations to solve accretion flows onto massive black holes (BHs) with a very high rate. Assuming that photon trapping limits the luminosity emerging from the central region to $L \lesssim L_{\text{Edd}}$, Inayoshi, Haiman & Ostriker (2016) have shown that an accretion flow settles to a “hyper-Eddington” solution, with a steady and isothermal ($T \simeq 8000$ K) Bondi profile reaching $\gtrsim 5000$ times the Eddington accretion rate $\dot{M}_{\text{Edd}} \equiv L_{\text{Edd}}/c^2$. Here we address the possibility that gas accreting with finite angular momentum forms a bright nuclear accretion disc, with a luminosity exceeding the Eddington limit ($1 \lesssim L/L_{\text{Edd}} \lesssim 100$). Combining our simulations with an analytic model, we find that a transition to steady hyper-Eddington accretion still occurs, as long as the luminosity remains below $L/L_{\text{Edd}} \lesssim 35 (M_{\text{BH}}/10^4 M_{\odot})^{3/2} (n_{\infty}/10^5 \text{ cm}^{-3}) (T_{\infty}/10^4 \text{ K})^{-3/2} (r_{\star}/10^{14} \text{ cm})^{-1/2}$, where n_{∞} and T_{∞} are the density and temperature of the ambient gas, and r_{\star} is the radius of the photosphere, at which radiation emerges. If the luminosity exceeds this value, accretion becomes episodic. Our results can be accurately recovered in a toy model of an optically thick spherical shell, driven by radiation force into a collapsing medium. When the central source is dimmer than the above critical value, the expansion of the shell is halted and reversed by ram pressure of the collapsing medium, and by shell’s weight. Our results imply that rapid, unimpeded hyper-Eddington accretion is possible even if the luminosity of the central source far exceeds the Eddington limit, and can be either steady or strongly episodic.

Key words: black hole physics, cosmology: theory, quasars: supermassive black holes

1 INTRODUCTION

The existence of bright high-redshift ($z \gtrsim 6$) quasars, powered by supermassive black holes (SMBHs) with $\gtrsim 10^{8-9} M_{\odot}$, poses questions about the formation and evolution of these SMBHs (Fan et al. 2003; Fan 2006; Willott et al. 2010; Mortlock et al. 2011; Venemans et al. 2013; Wu et al. 2015).

Several possible scenarios have been suggested for the origin of the SMBHs (Volonteri 2010; Haiman 2013; Johnson & Haardt 2016, references therein). One is remnant BHs of massive Population III (Pop III) stars with $\sim 100 M_{\odot}$ (Madau & Rees 2001; Haiman & Loeb 2001; Schneider et al. 2002; Islam, Taylor & Silk 2003; Volonteri, Haardt & Madau 2003; Tanaka & Haiman 2009). Second, the so-called direct collapse model (Loeb & Rasio 1994; Oh & Haiman 2002; Bromm & Loeb 2003; Begelman, Volonteri & Rees 2006; Lodato & Natarajan 2006; Shang, Bryan &

Haiman 2010; Schleicher et al. 2013; Regan, Johansson & Wise 2014; Inayoshi, Omukai & Tasker 2014; Visbal, Haiman & Bryan 2014; Alexander & Natarajan 2014; Pacucci & Ferrara 2015; Latif, Schleicher & Hartwig 2016; Chon et al. 2016) considers a more massive seed BH with $\sim 10^5 M_{\odot}$, formed by the collapse of a supermassive star (e.g., Begelman 2010; Hosokawa et al. 2013; Sakurai et al. 2016). Two direct-collapse BH candidates have recently been identified in the CANDELS/GOODS-S survey based on their very red expected spectra (Pacucci et al. 2016), and may be detected in the future through stellar tidal disruption events (Kashiyama & Inayoshi 2016). Thirdly, runaway collisions in star clusters produce massive stars which would be seeds for the SMBHs (e.g., Portegies Zwart et al. 2004; Omukai, Schneider & Haiman 2008; Devecchi & Volonteri 2009; Katz, Sijacki & Haehnelt 2015; Yajima & Khochfar 2016; Stone, Kuepper & Ostriker 2016).

How do seeds grow to SMBHs within the age of the universe at $z \gtrsim 6$? In any of the above seed formation models, subsequent BH growth needs to be still rapid (Tanaka

* sakurai@utap.phys.s.u-tokyo.ac.jp

2014). When the BH is fed by sufficiently strong gas flows, and the emergent luminosity increases, radiative feedback is likely to affect gas dynamics. Radiation force is crucially important at the vicinity of the BH horizon because the gas is highly opaque to electron scattering. In particular, if the luminosity approaches the Eddington luminosity, $L_{\text{Edd}} \equiv 4\pi cGM_{\text{BH}}/\kappa_{\text{es}}$, the radiation force becomes comparable to the gravity of the accreting BH and thus the accretion rate would be limited to the Eddington rate $\dot{M}_{\text{Edd}} \equiv L_{\text{Edd}}/c^2$. Note that starting with a $100(10^5) M_{\odot}$ seed BH, it takes $\simeq 0.7(0.4)$ Gyr to form a SMBH with $10^9 M_{\odot}$, assuming a continuous accretion at the Eddington rate with 10% radiative efficiency, i.e., $\dot{M} = 10 \dot{M}_{\text{Edd}}$. A massive seed thus eases the requirement on the duty cycle by a factor for $z \gtrsim 6$. However, “photon trapping” (Katz 1977; Begelman 1978) would help BHs grow at a higher rate than the Eddington rate. Photon trapping occurs when radiation within an optically thick flow is advected inwards by efficient electron scattering faster than it can escape via radiation diffusion. This then limits the emergent luminosity, and, in spherical symmetry, prevents it from exceeding the Eddington limit (Begelman 1979). The characteristic “trapping radius” is given by

$$R_{\text{tr}} \equiv \frac{\kappa_{\text{es}} \dot{M}}{4\pi c}, \quad (1)$$

outside which radiation escapes and contributes to the emergent luminosity. Thus, the maximum luminosity released by gravitational energy is estimated as $\simeq GM_{\text{BH}}\dot{M}/R_{\text{tr}} \sim L_{\text{Edd}}$. Numerical simulations have investigated rapid accretion with $\dot{M} \gg L_{\text{Edd}}/c^2$ and found that such high accretion rates are possible in a disk-like configuration, with radiation escaping vertically (e.g. Ohsuga et al. 2005; Sądowski et al. 2014; Jiang, Stone & Davis 2014; McKinney et al. 2014; Fragile, Olejar & Anninos 2014; Sądowski & Narayan 2016). Semi-analytical models also suggest the possibility of such rapid growth of SMBHs in the early Universe (e.g. Volonteri & Rees 2005; Madau, Haardt & Dotti 2014; Alexander & Natarajan 2014; Volonteri, Silk & Dubus 2015). Analytical arguments also support rapid growth via gas accretion at a super-Eddington rate (e.g. Pacucci, Volonteri & Ferrara 2015). A recent paper (Pezzulli, Valiante & Schneider 2016) shows that a high accretion rate of $\gtrsim 10^3 L_{\text{Edd}}/c^2$ is sustained at $z > 10$, even including a BH feedback model. On the other hand, radiation heating potentially suppresses gas inflows from larger scales where gas is not bounded by the BH gravity. The radiation heating effect from a BH makes the accretion behavior episodic and the averaged rate value is limited to $\lesssim 10\dot{M}_{\text{Edd}}$ (e.g. Ciotti & Ostriker 2001; Milosavljević, Couch & Bromm 2009; Park & Ricotti 2011, 2012; Park et al. 2016). To address this issue, we need to consider a *self-consistent solution of the accretion flow from larger scales where the gas accretion begins to small scales where photon trapping reduces the emergent luminosity*.

Recently, Inayoshi, Haiman & Ostriker (2016) (hereafter IHO16) has found a steady self-consistent spherically symmetric solution of gas accreting at a rate of $\gtrsim 5000 L_{\text{Edd}}/c^2$ (hereafter “hyper-Eddington accretion”) when

$$\left(\frac{n_{\infty}}{10^5 \text{ cm}^{-3}}\right) \gtrsim \left(\frac{M_{\text{BH}}}{10^4 M_{\odot}}\right)^{-1} \left(\frac{T_{\infty}}{10^4 \text{ K}}\right)^{3/2}, \quad (2)$$

where n_{∞} and T_{∞} are the density and temperature of the

ambient gas. They have shown that this condition corresponds to the HII region, generated by the ionizing radiation emerging from the photosphere, being smaller than the Bondi radius. For the hyper-Eddington case, the solution then consists of a radiation-dominated core, where photon trapping due to electron scattering is important, and an accreting envelope which follows an isothermal Bondi profile with $T \simeq 8000$ K. If photon trapping suppresses the luminosity, emerging from the photosphere, to below $\sim L_{\text{Edd}}$, radiation from the central region does not stop the gas accretion from larger scales. In fact, the size of the HII region remains much smaller than the Bondi radius, which results in a high inflow rate, unimpeded by radiation feedback.

However, IHO16 assumed that photon trapping is effective, and that the luminosity at the photosphere is limited to L_{Edd} . This assumption is not valid when the accretion flow with nonzero angular momentum produces a compact nuclear disk, potentially launching outflows or jets into polar regions (e.g., Ohsuga et al. 2005; Sądowski et al. 2014; McKinney et al. 2014). Photon trapping in the polar regions has also been found less efficient than in spherically symmetric flows, with magnetic buoyancy facilitating the vertical escape of radiation (Jiang, Stone & Davis 2014). As a result, the radiation luminosity in directions away from the disk plane can significantly exceed the Eddington luminosity.

In this paper, we investigate the impact of a high-luminosity central source, with $L > L_{\text{Edd}}$, on the spherical accretion flow at larger radii, by performing one-dimensional radiation hydrodynamical simulations. We show that the transition to steady hyper-Eddington accretion still occurs, as long as the radiation luminosity from the central bright source is as small as $L \lesssim 10 L_{\text{Edd}}$. This high-rate steady flow is maintained because the ram pressure of the infalling gas dominates the radiation force caused by the central nuclear disk. We also use a toy model of a momentum-driven shell embedded in a collapsing gas cloud, to demonstrate that the effect of the ram pressure significantly suppresses radiation feedback, in good agreement with our simulations.

This paper is organized as follows. In Section 2, we describe the setup of our simulations and the numerical methodology. We show the results of our simulations in Section 3 and give analytical arguments to explain the results in Section 4. In Section 5, we discuss our results and summarize our conclusions.

2 SIMULATION METHOD

2.1 Setup of the simulations

We solve structures of spherical accretion flows onto a BH with a mass of M_{BH} by performing one-dimensional hydrodynamical simulations which include radiative processes. Fig. 1 shows important physical scales of the gas structure. The Bondi radius is estimated analytically by

$$R_{\text{B}} = 1.98 \times 10^{18} M_{\text{BH},4} T_{\infty,4}^{-1} \text{ cm}, \quad (3)$$

within which the BH gravity exceeds the gas pressure and accretion begins. A photosphere forms at $R_{\text{ph}} \sim 10^{14-15}$ cm (IHO16) and the trapping radius (equation 1) is

$$R_{\text{tr}} = 1.48 \times 10^{12} M_{\text{BH},4} \dot{m}_3 \text{ cm}, \quad (4)$$

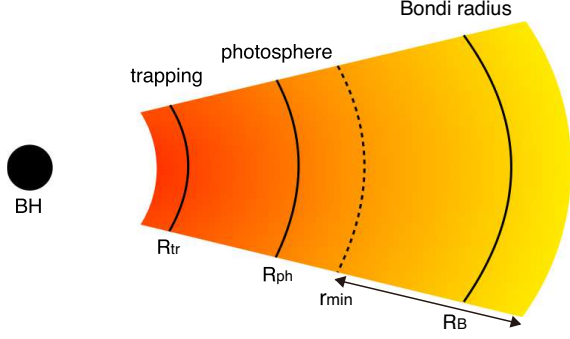


Figure 1. Schematic illustration of a spherically symmetric accretion flow onto a massive BH at a hyper-Eddington rate. The locations of the trapping radius R_{tr} , the photosphere R_{ph} and the Bondi radius R_{B} are shown. Our simulations solve for the structure of the accretion flow between $r_{\text{min}} (\simeq 10^{-3} R_{\text{B}}) \lesssim r \lesssim 10 R_{\text{B}}$.

where $M_{\text{BH},4} \equiv M_{\text{BH}}/(10^4 M_{\odot})$, $T_{\infty,4} \equiv T_{\infty}/(10^4 \text{ K})$ and $\dot{m}_3 \equiv (\dot{M}/\dot{M}_{\text{Edd}})/10^3$. It is desirable to resolve all these radii in the simulations in order to determine the structure of the flow self-consistently. However, this is computationally prohibitive, because both R_{tr} and R_{ph} are smaller than the Bondi radius by 4 – 5 orders of magnitude (see IHO16). In the following simulations, therefore we focus on the region between $10^{-3} R_{\text{B}} \lesssim r \lesssim 10 R_{\text{B}}$, and investigate whether hyper-Eddington accretion is realized without being impeded by radiation feedback. As a result, our simulation domain does not extend down to R_{tr} and R_{ph} . Instead, we set the emergent luminosity from the inner region by hand, using several different models of the radiation efficiency, including allowing for super-Eddington luminosities. Note that in our paper, we simply assume that the disc is small enough to be embedded well inside the inner-most radius of the simulation box and consider emerging radiation with $L > L_{\text{Edd}}$ from it.

2.2 Basic equations and numerical schemes

We use the hydrodynamical simulation code ZEUS (Stone & Norman 1992) to follow gas dynamics around the BH. For the spherically symmetric case, the continuity equation is given by

$$\frac{\partial \rho}{\partial t} + \frac{1}{r^2} \frac{\partial}{\partial r} (r^2 \rho v) = 0, \quad (5)$$

and the equation of motion is given by

$$\rho \left(\frac{\partial v}{\partial t} + v \frac{\partial v}{\partial r} \right) = -\frac{\partial p}{\partial r} - \rho \frac{\partial \Phi}{\partial r} + f_{\text{rad}}, \quad (6)$$

where ρ is the gas density, v is the velocity of the flow, p is the gas pressure, Φ is the gravitational potential of the BH, and f_{rad} is the radiation force per volume. We assume the gas pressure is given by the equation of state $p = (\gamma - 1)\rho e$, where $\gamma = 5/3$ and e is the specific energy density. For completeness, we adopt the general relativistic correction for the gravitational potential, $\Phi = -GM_{\text{BH}}/(r - R_{\text{Sch}})$ (Paczynski & Wiita 1980), although in practice these corrections are negligible in our simulation domain. The energy equation is given by

$$\rho \left(\frac{\partial e}{\partial t} + v \frac{\partial e}{\partial r} \right) = -p \frac{1}{r^2} \frac{\partial}{\partial r} (r^2 v) - \Lambda + \Gamma, \quad (7)$$

where Λ is the cooling rate and Γ is the heating rate. The cooling rate Λ includes the effect of the collisional excitation of H, He, He^+ atoms and by H free-free emission (Glover & Jappsen 2007):

$$\Lambda = \Lambda_{\text{H}} + \Lambda_{\text{He}} + \Lambda_{\text{He}^+} + \Lambda_{\text{ff}}. \quad (8)$$

The energy equation is solved by an implicit method, in order to stabilize the calculation.

We consider a chemical reaction network composed of the six primordial species of H, H^+ , He, He^+ , He^{++} and e^- . The number abundance of He nuclei relative to H nuclei is set to 8.33×10^{-2} . We consider the chemical reactions of photoionization, collisional ionization and radiative recombination of H, He, and He^+ . We adopt the on-the-spot approximation, i.e. recombination photons are quickly absorbed as ionizing photons and the recombinations to the ground state are ignored, and we use the case B recombination coefficient. The chemical reactions are solved for the six species with a semi-implicit formulation (Anninos et al. 1997). The electron fraction is derived from charge conservation.

The time step of the simulation is set to the minimum value among the Courant time, the cooling time and the chemical time, following Whalen & Norman (2006). We set the Courant number to be less than 0.5. The cooling time and chemical time are set to the minimum value of

$$t_{\text{cool}} \equiv 0.1 \frac{\rho e}{|\Lambda - \Gamma|}, \quad (9)$$

$$t_{\text{chem}} \equiv 0.01 \frac{x_e + 0.001 x_{\text{H}}}{x_e}, \quad (10)$$

on the grid, where x_e and x_{H} are the electron and neutral hydrogen fraction, respectively.

We solve steady and spherically symmetric radiation transfer equations to calculate the radiation force, the heating rates and photoionization rates. The steady assumption is valid because the cloud crossing time of photons ($\tau r/c$) is much shorter than the simulation time step. The transfer equation is given by

$$\frac{1}{r^2} \frac{d}{dr} (r^2 F_{\nu}) = 4\pi \eta_{\nu} - \rho \kappa_{\nu} c E_{\nu}, \quad (11)$$

where F_{ν} is the radiation flux, η_{ν} is the emissivity, κ_{ν} is the opacity and E_{ν} is the radiation energy density. The gas is optically thin against photons inside the ionized region and thus in those regions we approximate $F_{\nu} \approx c E_{\nu}$.

The photoionization rates k_i and the heating rates Γ_i ($i = \text{H}, \text{He}, \text{He}^+$) are calculated with a photon-conserving scheme (Whalen & Norman 2006)

$$k_i = \int_{\nu_i} \frac{4\pi \hat{J}_{\nu}}{h\nu} \sigma_i d\nu, \quad (12)$$

$$\Gamma_i = n_i \int_{\nu_i} \frac{4\pi \hat{J}_{\nu}}{h\nu} \sigma_i E_{\text{heat},i} d\nu, \quad (13)$$

where \hat{J}_{ν} is the mean intensity calculated to conserve the number of photons at each grid, σ_i is the cross section for bound-free absorption of ionizing photons, ν_i is the ionization energy, and $E_{\text{heat},i} = h\nu - h\nu_i$ is the excess energy of the photo-electron available for heating. The radiation force

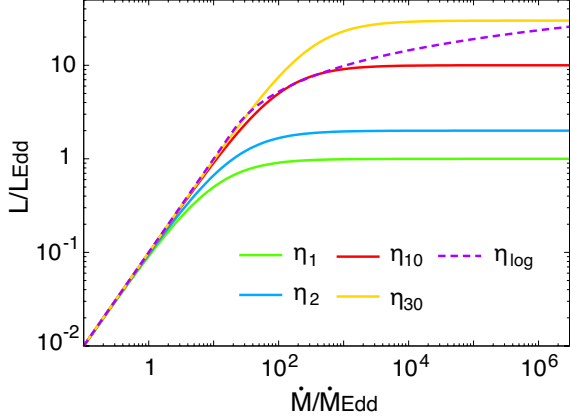


Figure 2. The bolometric luminosity assumed to be produced in the central regions, and enter our simulation domain at r_{\min} , as a function of the accretion rate $\dot{M}/\dot{M}_{\text{Edd}}$. Different curves correspond to the different adopted models of the radiative efficiency, $\eta_{f_{\text{Edd}}}$ with $1 \leq f_{\text{Edd}} \leq 30$ (solid curves) and η_{\log} (dashed curves).

due to electron scattering and bound-free transitions is calculated by

$$f_{\text{rad},i} = \frac{n_e}{c} \int \sigma_{\text{es}} F_\nu d\nu + \frac{\Gamma}{c} \quad (14)$$

where σ_{es} is the cross section for Thomson scattering.

The radiation flux entering the simulation domain at its inner boundary is specified by hand as follows. The radiation spectrum is assumed to be a single power-law of

$$F_{\nu,\text{in}} \propto \left(\frac{\nu}{\nu_{\min}} \right)^{-\alpha} \quad (\nu_{\min} \leq \nu \leq \nu_{\max}), \quad (15)$$

where ν_{\min} is the ionization threshold of neutral hydrogen, $h\nu_{\min} = 13.6$ eV, and $h\nu_{\max} \sim 30$ keV is the maximum cut-off frequency. The power-law index is set to $\alpha = 1.5$ (see IHO16). The normalization of the radiation flux is determined by $L = \eta \dot{M} c^2$, where \dot{M} is the mass flux through the innermost grid, η is the radiative efficiency, and L is the bolometric luminosity. We assume a simple model of the efficiency which mimics the effect of photon trapping for a high $\dot{m} (\gg 1)$ as

$$\eta_{f_{\text{Edd}}} \equiv \frac{1}{10 + \dot{m}/f_{\text{Edd}}}, \quad (16)$$

where $f_{\text{Edd}} \equiv L_{\text{max}}/L_{\text{Edd}}$ and L_{max} is the maximum luminosity for $\dot{m} \rightarrow \infty$ (see Fig. 2). In this model, the efficiency becomes a constant ($\eta \simeq 0.1$) for low \dot{m} , while $\eta \rightarrow f_{\text{Edd}}/\dot{m}$ for high \dot{m} . We do not consider an advection-dominated accretion flow (ADAF), because the accretion rates in our simulations do not drop below the critical value, $\dot{m} \approx 10^{-3}$ (Ichimaru 1977; Narayan & Yi 1994), at which a transition to ADAF would be expected (see Fig. 3). Note that IHO16 considered only the case with $f_{\text{Edd}} = 1$, where the luminosity never exceeds the Eddington luminosity. However, we here relax this assumption and allow super-Eddington luminosities. In addition to this model, we also consider a model of the efficiency which asymptotically approaches a logarithmic

form at high \dot{m} (Watarai et al. 2000),

$$\eta_{\log} = \begin{cases} 0.1 & (\dot{m} < 20) \\ \frac{2}{\dot{m}} \left[1 + \ln \left(\frac{\dot{m}}{20} \right) \right] & (\dot{m} > 20). \end{cases} \quad (17)$$

This prescription is motivated by the simulations with $\dot{m} \gg 1$, mentioned above, which find that photon trapping do not fully suppress the luminosity emerging from the central region (e.g., Jiang, Stone & Davis 2014; Sądowski et al. 2014).

We set spherical coordinates with a logarithmically-spaced grid in the radial direction as follows. The positions of the inner and outer boundary are set to r_{\min} and r_{\max} . The i -th grid is given by $r_i = r_{\min} + \Delta r_0 (\epsilon^{i-1} - 1)/(\epsilon - 1)$, where Δr_0 is the size of the inner-most grid and $\epsilon (= \Delta r_{i+1}/\Delta r_i)$ is the ratio between consecutive grids. For a given number of the grid-cells N , $\Delta r_0 = (r_{\max} - r_{\min})(\epsilon - 1)/(\epsilon^N - 1)$. Throughout this paper, we set $N = 700$, $\epsilon = 1.01$, $r_{\min} \sim 10^{-3} R_{\text{B}}$ and $r_{\max} = 5000 r_{\min}$ so that dynamics of gas accretion from outside the Bondi radius are calculated with sufficient resolution.

We adopt the “outflow” boundary condition (BC) at the innermost grid (e.g. Stone & Norman 1992). Under this BC, we set $v(r_{\min}) = v(r_{\min} + \Delta r_0)$ to avoid spurious reflection of wave energy at the boundary. However, when $L > L_{\text{Edd}}$, this BC artificially underestimates the effect of the radiation force on the innermost shell. This is because the velocity at r_{\min} , where the infalling gas should be significantly decelerated by radiation, is replaced by the velocity at $r_{\min} + \Delta r_0$, where deceleration is inefficient because radiation is partially absorbed by the gas at r_{\min} before reaching $r_{\min} + \Delta r_0$. To circumvent this underestimate, we adopt an alternative inner BC: $v(r_{\min} + \Delta r_0) = v(r_{\min})$ for $L > L_{\text{Edd}}$. When we use this BC, we choose the size of the innermost grid so that the gas element at $[r_{\min}, r_{\min} + \Delta r_0]$ is optically thick to electron scattering ($\tau_{\text{es}} \gtrsim 1$). If we chose a small grid size of Δr_0 so that $\tau_{\text{es}} \ll 1$, most of radiation should penetrate to the second grid and cause significant deceleration there. This would be missed by the new BC of $v(r_{\min} + \Delta r_0) = v(r_{\min})$, which would then again underestimate the effect of radiation force. We have checked that $\tau_{\text{es}} \gtrsim 1$ at $r = r_{\min} + \Delta r_0$ is ensured for $N = 700$.

3 RESULTS

Fig. 3 shows the time evolution of the accretion rate for several models of the radiative efficiency $\eta_{f_{\text{Edd}}}$ ($1 \leq f_{\text{Edd}} \leq 30$) (solid curves) and η_{\log} (dashed curve). We here set the BH mass to $M_{\text{BH}} = 2 \times 10^4 M_{\odot}$ and adopt an initially neutral uniform gas with $n_{\infty} = 10^5 \text{ cm}^{-3}$, $T_{\infty} = 10^4 \text{ K}$ and $v = 0$. The dotted curve presents the evolution with radiation off at the inner boundary, approaching the Bondi rate,

$$\frac{\dot{M}_{\text{B}}}{\dot{M}_{\text{Edd}}} = 7.3 \times 10^3 M_{\text{BH},4} n_{\infty,5} T_{\infty,4}^{-3/2}, \quad (18)$$

where we estimate the Bondi rate for the isothermal case, $\dot{M}_{\text{B}} = e^{3/2} \pi \rho_{\infty} R_{\text{B}}^2 c_{\infty}$. With radiation on for $f_{\text{Edd}} = 1$, the accretion rate is much lower than the case without radiation. The average rate is limited to $\sim 20 \dot{M}_{\text{Edd}}$ at $t < 10^5 \text{ yr}$, where the luminosity from the central region is $\sim 0.7 L_{\text{Edd}}$. At $t \gtrsim 1.3 \times 10^5 \text{ yr}$, the accretion rate becomes episodic

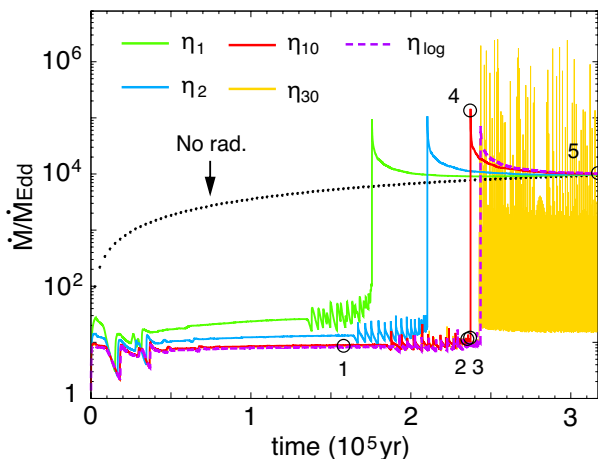


Figure 3. Time evolution of the accretion rates for the five different models of radiative efficiency shown in Fig. 2 (and for $M_{\text{BH}} = 2 \times 10^4 M_{\odot}$, $n_{\infty} = 10^5 \text{ cm}^{-3}$ and $T_{\infty} = 10^4 \text{ K}$). The dotted curve shows the time evolution of the rate in the absence of any radiation (settling to the Bondi rate). Circles mark five different epochs, at which we show radial profiles for the model of η_{10} in Fig. 4.

and increases promptly to a higher value, which we call the transition. This result is consistent with that found in IHO16 (see their Fig. 5). After the transition, the accretion rate approaches the Bondi rate. The hyper-Eddington accretion is realized because the HII region is always confined inside the Bondi radius, i.e. $R_{\text{HII}} \lesssim R_{\text{B}}$ (see below and §4).

For moderately larger values of $1 < f_{\text{Edd}} \leq 10$, we find the same transition to steady hyper-Eddington accretion as in $f_{\text{Edd}} = 1$. Even in these cases, the luminosity before the transition is limited to $\sim L_{\text{Edd}}$. The transition time is delayed for higher f_{Edd} because radiation force is non-negligible, and contributes an outward-directed force on the gas. After the transition, the luminosity exceeds the Eddington luminosity. However, the hyper-Eddington accretion is maintained since the ram pressure overcomes the radiation force at the innermost region. Note that the result in the model with η_{log} (equation 17) does not change qualitatively because the luminosity after the transition ($L \lesssim 20 L_{\text{Edd}}$) is as small as in the cases with $1 < f_{\text{Edd}} \leq 10$.

For the highest value of $f_{\text{Edd}} = 30$, the transition to a hyper-Eddington phase occurs, but the behavior of the accretion rate is different from the other cases after the transition. Namely, the accretion rate is unstable, and begins to oscillate at the innermost grid. In this case, radiation force with $L \simeq 30 L_{\text{Edd}}$ from the central region prevents a steady accretion flow from being realized. However, the radiation force does not suppress the gas accretion in the quiescent phases. As a result, the time-averaged accretion rate still matches the Bondi rate. This implies that the central BH grows rapidly even for $f_{\text{Edd}} \gtrsim 30$ (see discussion in §5). This critical luminosity to maintain steady hyper-Eddington accretion is determined by a comparison of the radiation force with the ram pressure and gravity of the infalling gas (see Section 4.1 below).

Fig. 4 shows radial profiles of the gas density, temperature, and local mass inflow rate $\dot{M} = 4\pi r^2 \rho |v|$ for the model with $f_{\text{Edd}} = 10$ at five different epochs corresponding to the

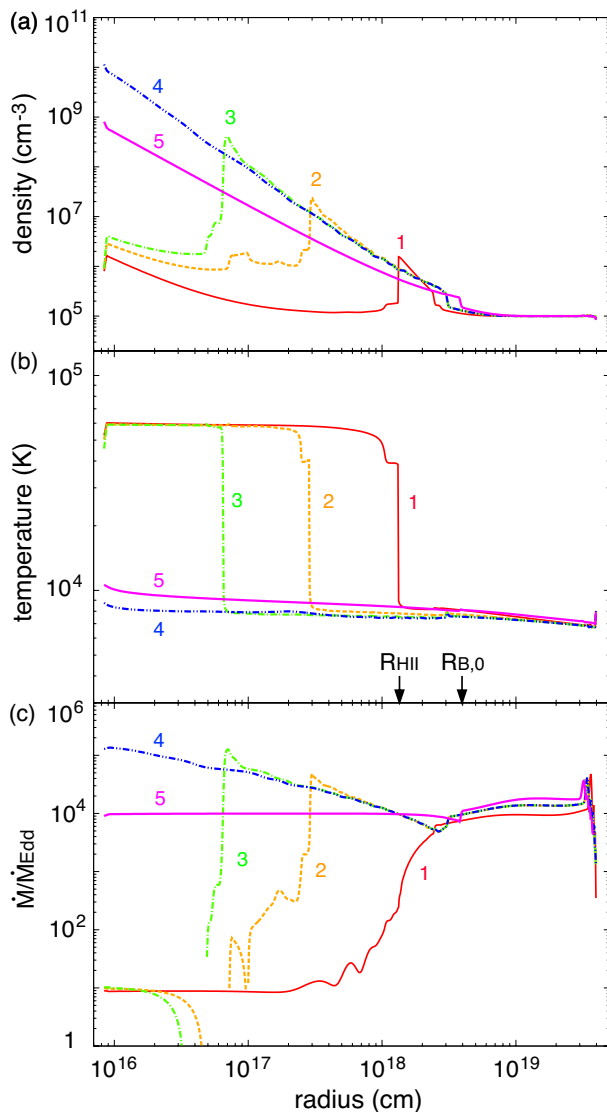


Figure 4. Radial profiles of the density, temperature and local accretion rate for the model of η_{10} (see equation 16) at the five different epochs shown by circles in Fig. 3. The five curves correspond to (i) $t = 1.58 \times 10^5 \text{ yr}$ (red), (ii) $2.35 \times 10^5 \text{ yr}$ (orange), (iii) $2.371 \times 10^5 \text{ yr}$ (green), (iv) $2.373 \times 10^5 \text{ yr}$ (blue) and (v) $3.17 \times 10^5 \text{ yr}$ (magenta). In panel (b), the size of the HII region R_{HII} and the initial Bondi radius $R_{\text{B},0}$ are shown. In this case, the condition required for steady hyper-Eddington accretion, $R_{\text{HII}} \lesssim R_{\text{B},0}$, is satisfied.

filled circles in Fig. 3. As IHO16 discussed, the condition required for hyper-Eddington accretion is given by equation (2), which is equivalent to the condition that the size of the HII region is smaller than the initial Bondi radius (see also §4.1). Fig. 4(b) shows that the condition is satisfied for this case ($R_{\text{HII}} < R_{\text{B},0}$). The physical explanation why this transition occurs are as follows. When the accretion occurs, the HII region expands to the radius of R_{HII} , within which radiation force and gas pressure suppress the gas accretion. However, since $R_{\text{HII}} < R_{\text{B},0}$, the accreting gas accumulates in the region $R_{\text{HII}} \lesssim r \lesssim R_{\text{B}}$ (curve 1 in Fig. 4a). Once this shell becomes sufficiently dense and massive, it begins to fall inward due to the gravitational force of the central

BH (curves 2 and 3 in Fig. 4a). Concurrently, the HII region shrinks and the accretion rate increases (curve 4 in Figs. 4b and c). After the transition, the gas profile approaches a steady and isothermal Bondi profile with $\rho \propto r^{-3/2}$ and $T \simeq 8000$ K (curve 5 in Fig. 4).

For the case with $f_{\text{Edd}} = 30$, radial profiles of the gas properties are almost identical to those for $f_{\text{Edd}} = 10$, except inside a narrow central HII region. In this case, the strong radiation force eventually blows the ionized gas outward. However, once the luminosity decreases due to suppression of the gas accretion, ram pressure caused by rapid accretion from outside the HII region pushes the ejected gas inward again, resulting in episodic accretion. This result also shows that as long as $R_{\text{HII}} < R_{\text{B},0}$ is satisfied, the time-averaged accretion rate should match the steady hyper-Eddington Bondi rate, even for $f_{\text{Edd}} = 30$.

Finally, we ran a separate, simpler suite of simulations, as an academic exercise, to further clarify the effect of radiation force with a super-Eddington luminosity on the accretion flow. In the above simulations, the luminosity is coupled with the accretion rate. Instead, we here assume a steady and isothermal Bondi accretion flow as the initial condition, and turn on the central source with a *constant* luminosity, independent from the accretion rate. This setup allows us to compare the results directly with a toy model, discussed in §4.2 below. Fig. 5 shows two cases for $L = 10 L_{\text{Edd}}$ (red solid) and $30 L_{\text{Edd}}$ (blue dashed). For $L = 10 L_{\text{Edd}}$, the gas accretion does not change at all after the radiation turns on at $t = 0$. On the other hand, for $L = 30 L_{\text{Edd}}$, the radiation force is so strong that the gas inflow is decelerated and shuts off. This behaviour differs from the previous case with $f_{\text{Edd}} = 30$ (see Fig. 3), in which the radiation force was set to depend on the accretion rate, and accretion was episodic, rather than being shut off.

4 ANALYTIC ARGUMENTS

As we have shown in §3, a transition to a steady hyper-Eddington accretion occurs for $M_{\text{BH}} = 2 \times 10^4 M_{\odot}$ and $n_{\infty} = 10^5 \text{ cm}^{-3}$, as long as the maximum luminosity from the central region is $L/L_{\text{Edd}} (= f_{\text{Edd}}) \lesssim 20$. Although a steady accretion is replaced by strongly fluctuating, episodic accretion for $f_{\text{Edd}} \geq 30$, the time-averaged rate remains close to the Bondi rate. We discuss the physical interpretation of these results with a toy model of an optically thick spherical shell, driven by radiation force from a central source.

4.1 Hyper-Eddington accretion conditions

As we explain in §3 (see also IHO16), the transition to hyper-Eddington accretion occurs when the Bondi radius $R_{\text{B}} (\propto M_{\text{BH}} T_{\infty}^{-1})$ is larger than the size of the HII region R_{HII} . The latter is estimated by the balance between photoionization and radiative recombination as

$$R_{\text{HII}} = \left(\frac{3Q_{\text{ion}}}{4\pi n_{\infty}^2 \alpha_{\text{B}}} \right)^{1/3}, \quad (19)$$

where Q_{ion} is the mean number of ionizing photons emitted per unit time and α_{B} is the case B recombination rate. Since we consider the power-law spectrum with the index of -1.5 , we obtain $Q_{\text{ion}} = L/(3h\nu_{\text{min}})$. Before the transition occurs,

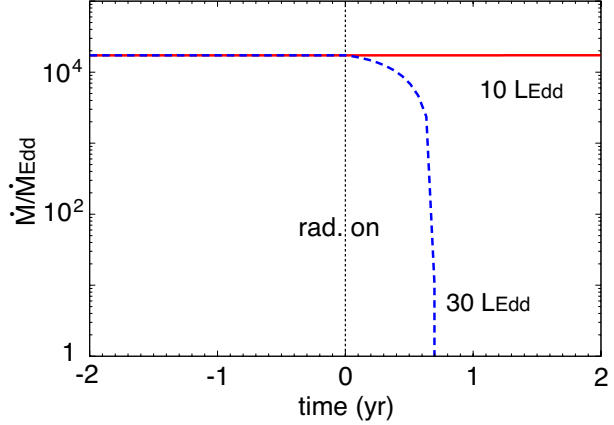


Figure 5. The effect of radiation force from a constant luminosity source on an initially steady and isothermal Bondi accretion flow. At $t = 0$, we turn on the radiation with $L = 10 L_{\text{Edd}}$ (red solid) or $L = 30 L_{\text{Edd}}$ (blue dashed). In the former case, the accretion rate does not change from the Bondi rate, while in the latter case, the accretion is shut off by radiation force.

the luminosity is limited to $\sim L_{\text{Edd}}$ (see Figs. 2 and 3). Thus, since $R_{\text{HII}} \propto L_{\text{Edd}}^{1/3} n_{\infty}^{-2/3} \propto M_{\text{BH}}^{1/3} n_{\infty}^{-2/3}$, the transition condition of $R_{\text{B}} > R_{\text{HII}}$ is written as equation (2) where we set the temperature within the HII region to 6×10^4 K. Note that for the evaluation of R_{HII} we here assume the constant density profile with n_{∞} instead of the Bondi density profile, which is actually realized just before the transition. The resulting value of R_{HII} from Eq. (19) is larger by a factor of a few than the actual value because equation (19) neglects the fact that the density profile has a steep slope ($\rho \propto r^{-\beta}$; $0 < \beta < 3/2$). Thus, our assumption of a constant density profile is rather conservative in terms of the conditions for hyper-Eddington accretion.

After the transition, the radiation luminosity from the central BH in certain directions would be brighter than $\sim L_{\text{Edd}}$ (e.g. Ohsuga et al. 2005; Sądowski et al. 2014; Jiang, Stone & Davis 2014). In the standard picture of outflows driven by radiation force with $L > L_{\text{Edd}}$, hyper-Eddington accretion seems unlikely to occur because radiation force due to electron scattering dominates the BH gravity. However, in our case, all momentum of the radiation is essentially absorbed by neutral hydrogen at the edge of the HII region within a short mean-free path. As a result, the radiation force, exerted on the recombination shell near R_{HII} is in fact *larger* than that onto ionized gas by a factor of $1/\tau_{\text{e}}$, where $\tau_{\text{e}} \sim n\sigma_{\text{T}}R_{\text{HII}} (\lesssim 1)$. On the other hand, the radiation has no impact outside the HII region, where rapid hyper-Eddington inflow can develop. As a result, a large ram pressure is exerted inward at the boundary of the HII region, which can significantly exceed the gravity of the BH. Furthermore, the infalling gas can accumulate near R_{HII} and increase the inward gravitational force. Therefore, the usual calculation of the Eddington limit, which equates radiation force on electrons with the BH's gravity, must be replaced in our case by a comparison between the (larger) radiation force on the neutral HI and the (larger) inward ram pressure and gravity.

When the ram pressure dominates the radiation force even after the transition, a steady hyper-Eddington accretion is maintained. The stability condition is written as

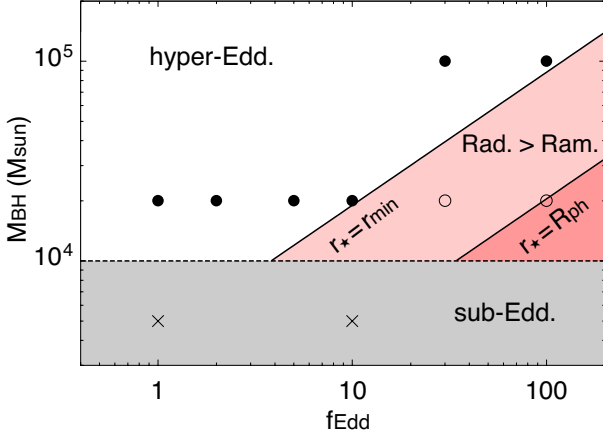


Figure 6. Summary of three different accretion regimes, occurring for different values of f_{Edd} and M_{BH} . Dashed and solid lines show the conditions given by Eqs. (2) and (20) for $n_{\infty} = 10^5 \text{ cm}^{-3}$, $T_{\infty} = 10^4 \text{ K}$, respectively. For the solid lines, we show two cases with the central radiation emerging from $r_{\star} = r_{\text{min}}$ (the inner boundary of the simulations) or from R_{ph} (the expected location of the photosphere). Different symbols mark simulation runs in which steady hyper-Eddington accretion was realized (filled circles), accretion became strongly episodic due to radiation force (open circles), and the transition to hyper-Eddington flow was suppressed entirely because of radiation heating and ionization (crosses).

$\dot{M}_{\text{B}}|v| > L/c$ at $r = r_{\star}$ where all radiation is absorbed. Since the inflow velocity is set to $|v| = (2GM_{\text{BH}}/r)^{1/2}$ at $r \geq r_{\star}$, we obtain

$$f_{\text{Edd}} = \frac{L}{L_{\text{Edd}}} \lesssim 11 M_{\text{BH},4}^{3/2} n_{\infty,5} T_{\infty,4}^{-3/2} r_{\star,15}^{-1/2}, \quad (20)$$

where $r_{\star,15} = r_{\star}/(10^{15} \text{ cm})$. As a conservative estimate, we set $r_{\star} = r_{\text{min}} (= 8 \times 10^{15} \text{ cm})$. For the case with $M_{\text{BH},4} = 2$, $n_{\infty,5} = 1$ and $T_{\infty,4} = 1$, hyper-Eddington accretion remains stable as long as $f_{\text{Edd}} \lesssim 10$. This estimate agrees with our simulation results shown in §3. In practice, the radiation should emerge from the photosphere located at a smaller radius, $R_{\text{ph}} (< r_{\text{min}})$. Although our simulations do not resolve the photosphere, if we adopt $R_{\text{ph}} \simeq 10^{14} \text{ cm}$ (shown in Fig. 11 of IHO16), we find the critical luminosity of $f_{\text{Edd}} \lesssim 100$. We discuss this critical luminosity further, using a simple toy model, in §4.2 below.

We summarize the necessary conditions for hyper-Eddington accretion in Figs. 6 and 7. The conditions of equations (20) (solid) and (2) (dashed) are shown in the $f_{\text{Edd}} - M_{\text{BH}}$ and $f_{\text{Edd}} - n_{\infty}$ planes, respectively. For the solid lines, we have set either $r_{\star} = r_{\text{min}}$ or $r_{\star} = R_{\text{ph}}$. Below the dashed lines, hyper-Eddington accretion is not realized because of radiation heating and ionization (cross; sub-Edd.). In the region between the solid and dashed lines, the hyper-Eddington accretion could occur but a steady state is not achieved because of radiation force dominating ram pressure and gravity (open circle; Rad. > Ram.). Only in the region above those lines, a steady hyper-Eddington accretion is allowed (filled circle; Hyper-Edd.).

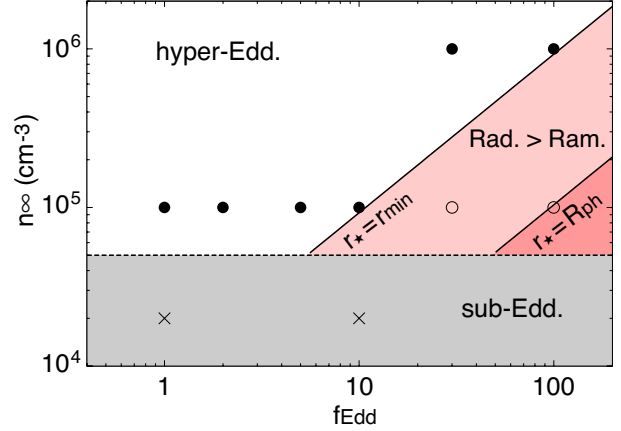


Figure 7. Same figure as Fig. 6 but for f_{Edd} and n_{∞} . We set $M_{\text{BH}} = 2 \times 10^4 M_{\odot}$ and $T_{\infty} = 10^4 \text{ K}$.

4.2 1D model for a momentum-driven shell

In order to understand the physics which allows hyper-Eddington accretion, we consider a toy model of a geometrically thin, but optically thick spherical shell around a point source, driven by radiation force into a rapidly collapsing medium (e.g. King 2003; Kasliwal, Lovelace & Houck 2005). The luminosity L of the central source is assumed constant, and the equation of motion of the shell is given by

$$\frac{d}{dt}(M_{\text{sh}} \dot{R}_{\text{sh}}) = \frac{L}{c} - \dot{M}(|v| + \dot{R}_{\text{sh}}) - \frac{GM_{\text{BH}}M_{\text{sh}}}{R_{\text{sh}}^2}, \quad (21)$$

where M_{sh} is the mass of the shell, R_{sh} is the distance of the shell from the center, and \dot{M} and v are the accretion rate and velocity of the gas inflow just outside the shell. The terms on the right hand side correspond to the outward force exerted on the shell by radiation force, and the inward forces due to ram pressure of the rapid inflow and the BH's gravity. We here assume that (i) the shell is optically thick to the UV (ionizing) radiation and absorbs all incident radiation with momentum of L/c , and that (ii) the entire cloud is effectively optically thin to the recombination radiation. If the recombination radiation is efficiently scattered by the neutral shell, that is, if condition (ii) is invalid, then the radiation is trapped within the shell (i.e. the neutral shells just outside the HII region). Multiple scattering events in this regime would increase the total radiation pressure force to $\simeq \tau_{\text{scat}} L/c$, where τ_{scat} is an effective optical depth to scattering. In our case, HI Rayleigh scattering is negligible, but Ly α scattering would be important because of the high optical depth at the line center, $\tau_{\text{Ly}\alpha} \sim 10^{10} - 10^{12}$. However, before radiation pressure by Ly α affects motion of the shell, the Ly α photons would be converted to $2S \rightarrow 1S$ continuum photons and $\sim 1 \text{ eV}$ photons (H^- free-bound transition), to which the shell is optically thin. We therefore expect our condition (ii) to hold, with an effective scattering opacity τ_{scat} at most a factor of a few. However, future work is needed to investigate the effect of the trapping of Ly α radiation, its conversion to lower-energy continuum photons, and the escape of these photons from the clouds.

The growth rate of the shell is given by

$$\frac{dM_{\text{sh}}}{dt} = \dot{M} \left(1 + \frac{\dot{R}_{\text{sh}}}{|v|} \right), \quad (22)$$

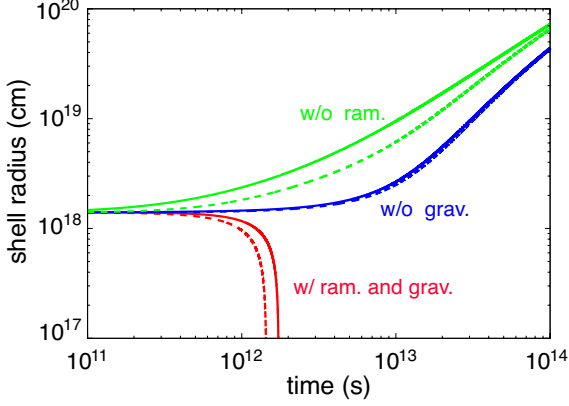


Figure 8. Time evolution of a geometrically thin, optically thick shell, driven by the radiation force of a central source into a rapidly collapsing cloud. The evolution is from a toy model that incorporates the outward radiation force, as well as the inward ram pressure and gravitational forces on the shell, initially located at $R_{\text{sh},0} = R_{\text{HI}} (\simeq 1.4 \times 10^{18} \text{ cm})$. Each curve corresponds to the case with both ram pressure and gravity (red), and with either gravity (blue) or ram pressure (green) artificially turned off. In each case, the initial density profile was assumed to be either constant (solid) or to follow the Bondi profile (dashed; Eq. 24). We set $f_{\text{Edd}} = 1$, $\dot{M} = \dot{M}_{\text{B}}$, $M_{\text{BH}} = 2 \times 10^4 M_{\odot}$, $n_{\infty} = 10^5 \text{ cm}^{-3}$ and $T_{\infty} = 10^4 \text{ K}$. This shell corresponds to that shown in phase (i) in Fig. 4(a).

and the initial shell mass is given by

$$M_{\text{sh},0} = \int_0^{R_{\text{sh},0}} 4\pi r^2 \rho(r) dr, \quad (23)$$

where the subscript 0 means the initial value. For simplicity, we consider two extreme cases for the density profile: a constant density profile $\rho(r) = \text{const.}$ and the Bondi profile $\rho(r) \propto r^{-3/2}$, with corresponding initial masses of

$$M_{\text{sh},0} = \begin{cases} \frac{4}{3} \pi R_{\text{sh},0}^3 \rho_{\infty} & \text{for } \rho(r) = \rho_{\infty}, \\ \frac{8}{3} \pi R_{\text{B}}^{3/2} R_{\text{sh},0}^{3/2} \rho_{\infty} & \text{for } \rho(r) = \rho_{\infty} \left(\frac{r}{R_{\text{B}}} \right)^{-3/2}. \end{cases} \quad (24)$$

We here set $\dot{M} = \dot{M}_{\text{B}}$, the free-fall velocity $|v| = (2GM_{\text{BH}}/r)^{1/2}$, $\dot{R}_{\text{sh},0} = 0$, $M_{\text{BH}} = 2 \times 10^4 M_{\odot}$, $n_{\infty} = 10^5 \text{ cm}^{-3}$ and $T_{\infty} = 10^4 \text{ K}$.

First, we consider time evolution of a dense shell which initially stalls at $R_{\text{sh},0} = R_{\text{HI}} (\simeq 1.4 \times 10^{18} \text{ cm})$ before the transition to hyper-Eddington accretion occurs, when $L \simeq L_{\text{Edd}} (f_{\text{Edd}} \simeq 1)$. This shell corresponds to that shown in Fig. 4(a) (phase 1). Fig. 8 shows three cases, in which the ram pressure of the inflowing gas and the BH's gravity on the accumulated mass of the shell are both included (red), and in which either the gravity (blue) or the ram pressure (green) are artificially turned off. Solid (dashed) curves correspond to constant (Bondi) initial density profiles. As this figure shows, when both ram pressure and gravity are included, the shell radius contracts. On the other hand, when either of the inward forces are turned off the shell continues to expand, and never accretes onto the center. Note that the expansion velocity of the shell is slower for the cases with heavier masses (dashed), but the choice of the initial shell

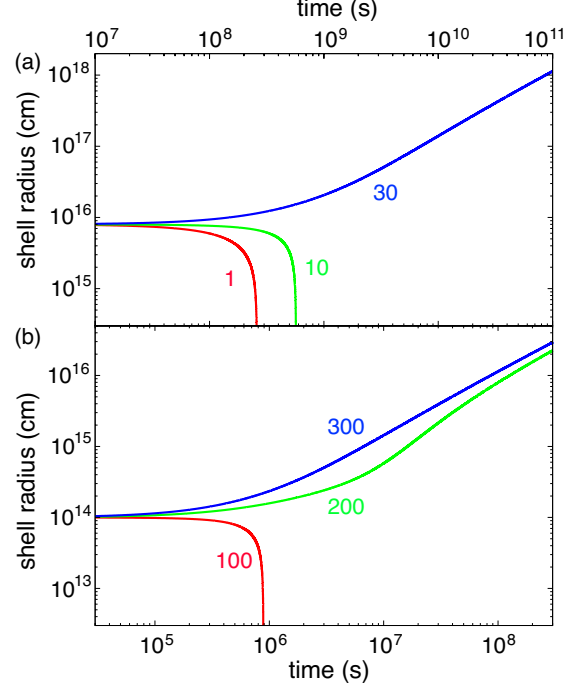


Figure 9. Same as Fig. 8 but for different values of $R_{\text{sh},0}$ and f_{Edd} . The initial shell radii and f_{Edd} are set to (a) $R_{\text{sh},0} = r_{\text{min}} (= 8 \times 10^{15} \text{ cm})$ and $f_{\text{Edd}} = 1$ (red), 10 (green) and 30 (blue) or to (b) $R_{\text{sh},0} = R_{\text{ph}} (\simeq 10^{14} \text{ cm})$ and $f_{\text{Edd}} = 100$ (red), 200 (green) and 300 (blue). The initial shell mass is computed for a constant density profile, and the effects of ram pressure and gravity are both included.

mass is not important. Overall, we infer that it is the combination of the ram pressure and gravity that overwhelms radiation force and yields hyper-Eddington accretion. The role of ram pressure is found to be somewhat more important (the shell expands faster without ram pressure [green] than without gravity [blue]).

Next, Fig. 9(a) shows the time evolution of a shell initially located at $R_{\text{sh},0} = r_{\text{min}} (= 8 \times 10^{15} \text{ cm})$, for $f_{\text{Edd}} = 1$ (red), 10 (green) and 30 (blue). These correspond to the cases after hyper-Eddington accretion is realized in the simulations. We here estimate the initial shell mass assuming a constant density profile, and the effects of ram pressure and gravity are both included. Fig. 9(a) clearly shows that for $f_{\text{Edd}} \lesssim 10$, the shell contracts within 20 yr, resulting in hyper-Eddington accretion. This result is in excellent agreement with our simulations and analytical arguments in §4.1. Fig. 9(b) also shows the case for the initial shell radius of $R_{\text{sh},0} = R_{\text{ph}} (\simeq 10^{14} \text{ cm})$, for $f_{\text{Edd}} = 100$ (red), 200 (green) and 300 (blue). The shell can contract for $f_{\text{Edd}} \lesssim 100$, which is again in agreement with the results shown in Figs. 6 and 7.

5 SUMMARY AND DISCUSSIONS

We have performed one-dimensional radiation hydrodynamical simulations to solve spherically symmetric accretion flows onto massive BHs with a very high rate. Our setup extends simulations in our earlier work IHO16, by allowing the central luminosity to exceed the Eddington luminosity

($1 \lesssim L/L_{\text{Edd}} \lesssim 100$). This is motivated by the possibility of gas accreting with finite angular momentum, and forming a bright nuclear disc, fed at rates well in excess of the Eddington rate (e.g. Ohsuga et al. 2005; Sądowski et al. 2014; Jiang, Stone & Davis 2014; McKinney et al. 2014).

We find that a transition to hyper-Eddington accretion phase occurs when

$$\dot{M} \gtrsim 5000 \dot{M}_{\text{Edd}} = 5000 L_{\text{Edd}}/c^2, \quad (25)$$

(see also equation 2). This condition remains identical to that found by IHO16 who assume that photon trapping effectively limits the emerging luminosity to $\lesssim L_{\text{Edd}}$. However, we identify a new condition, which determines whether the hyper-Eddington accretion is steady, or strongly episodic. We find that a steady state is maintained as long as the radiation luminosity from the central source is below a critical value,

$$\frac{L}{L_{\text{Edd}}} \lesssim 11 \left(\frac{M_{\text{BH}}}{10^4 M_{\odot}} \right)^{3/2} \left(\frac{n_{\infty}}{10^5 \text{ cm}^{-3}} \right). \quad (26)$$

This corresponds to the requirement that the ram pressure of the collapsing medium and the BH gravity on the accumulated mass of the shell at the edge of the HII region dominate over the radiation force, i.e. $\dot{M}|v| \gtrsim L/c$ (see equation 20). If the luminosity exceeds this critical value, then a steady hyper-Eddington phase can not exist, and the accretion instead becomes episodic. The time-averaged rate still matches the unimpeded Bondi rate, \dot{M}_{B} , provided that the condition in Eq. 25 is satisfied. We summarize the three different types of accretion flows, determined by the above two conditions, in Figs. 6 and 7. In this paper, we also offered a physical understanding of our simulation results: we showed that the latter can be recovered in a toy model of an optically thick spherical shell, driven by radiation into a collapsing cloud.

Throughout this paper, we have assumed a single power-law radiation spectrum with an index of $\alpha = -1.5$ over a frequency range of $13.6 \text{ eV} \leq h\nu \leq 30 \text{ keV}$ (see equation 15). In this case, all of the radiation can contribute to ionization of neutral gas. However, a realistic spectrum of an accretion disk around a BH would allow lower energy photons with $h\nu < 13.6 \text{ eV}$ which can escape without ionizing the accreting gas (e.g., Tanaka & Menou 2010). Thus, assuming a realistic spectrum, but with a fixed total luminosity, the transition to hyper-Eddington accretion is more likely to occur, compared to our case.

In our simulations, the photosphere and trapping radius, located at small radii, are not resolved directly. When the accreting gas has a finite angular momentum, a compact accretion disk should form around the central BH. Then, anisotropic radiation and/or outflows/jets from the center would break the spherical symmetry of the inflow, at least in the inner regions. A fully self-consistent treatment of such an accretion flow, which has an anisotropic, bright source with $L > L_{\text{Edd}}$ at the central region, embedded in a quasi-spherical inflow at large radii, will require multi-dimensional radiation hydrodynamical simulations.

6 ACKNOWLEDGEMENTS

Yuya Sakurai thanks the Columbia University Astronomy Department for its hospitality during an extended

visit, during which this work was completed. We thank Mark Dijkstra, Jeremiah P. Ostriker and Naoki Yoshida for fruitful discussions. This work is partially supported by Advanced Leading Graduate Course for Photon Science (YS), by Grant-in-Aid for JSPS Fellows (15H00776: YS), by the Simons Foundation through the Simons Society of Fellows (KI), and by NASA grants NNX11AE05G and NNX15AB19G (ZH). Numerical computations were carried out on a PC cluster at the Center for Computational Astrophysics of the National Astronomical Observatory of Japan.

REFERENCES

- Alexander T., Natarajan P., 2014, *Science*, 345, 1330
 Anninos P., Zhang Y., Abel T., Norman M. L., 1997, *New Astronomy*, 2, 209
 Begelman M. C., 1978, *MNRAS*, 184, 53
 Begelman M. C., 1979, *MNRAS*, 187, 237
 Begelman M. C., 2010, *MNRAS*, 402, 673
 Begelman M. C., Volonteri M., Rees M. J., 2006, *MNRAS*, 370, 289
 Bromm V., Loeb A., 2003, *ApJ*, 596, 34
 Chon S., Hirano S., Hosokawa T., Yoshida N., 2016, [arXiv:1603.08923](https://arxiv.org/abs/1603.08923)
 Ciotti L., Ostriker J. P., 2001, *ApJ*, 551, 131
 Devecchi B., Volonteri M., 2009, *ApJ*, 694, 302
 Fan X., 2006, *New A. Rev.*, 50, 665
 Fan X. et al., 2003, *AJ*, 125, 1649
 Fragile P. C., Olejar A., Anninos P., 2014, *ApJ*, 796, 22
 Glover S. C. O., Jappsen A.-K., 2007, *ApJ*, 666, 1
 Haiman Z., 2013, in *Astrophysics and Space Science Library*, Vol. 396, *The First Galaxies*, Wiklind T., Mobasher B., Bromm V., eds., p. 293
 Haiman Z., Loeb A., 2001, *ApJ*, 552, 459
 Hosokawa T., Yorke H. W., Inayoshi K., Omukai K., Yoshida N., 2013, *ApJ*, 778, 178
 Ichimaru S., 1977, *ApJ*, 214, 840
 Inayoshi K., Haiman Z., Ostriker J. P., 2016, *MNRAS*, 459, 3738
 Inayoshi K., Omukai K., Tasker E., 2014, *MNRAS*, 445, L109
 Islam R. R., Taylor J. E., Silk J., 2003, *MNRAS*, 340, 647
 Jiang Y.-F., Stone J. M., Davis S. W., 2014, *ApJ*, 796, 106
 Johnson J. L., Haardt F., 2016, [arXiv:1601.05473](https://arxiv.org/abs/1601.05473)
 Kashiyama K., Inayoshi K., 2016, [arXiv:1602.04293](https://arxiv.org/abs/1602.04293)
 Kasliwal M. M., Lovelace R. V. E., Houck J. R., 2005, *ApJ*, 630, 875
 Katz H., Sijacki D., Haehnelt M. G., 2015, *MNRAS*, 451, 2352
 Katz J. I., 1977, *ApJ*, 215, 265
 King A., 2003, *ApJ*, 596, L27
 Latif M. A., Schleicher D. R. G., Hartwig T., 2016, *MNRAS*, 458, 233
 Lodato G., Natarajan P., 2006, *MNRAS*, 371, 1813
 Loeb A., Rasio F. A., 1994, *ApJ*, 432, 52
 Madau P., Haardt F., Dotti M., 2014, *ApJ*, 784, L38
 Madau P., Rees M. J., 2001, *ApJ*, 551, L27
 McKinney J. C., Tchekhovskoy A., Sądowski A., Narayan R., 2014, *MNRAS*, 441, 3177
 Milosavljević M., Couch S. M., Bromm V., 2009, *ApJ*, 696, L146
 Mortlock D. J. et al., 2011, *Nature*, 474, 616
 Narayan R., Yi I., 1994, *ApJ*, 428, L13
 Oh S. P., Haiman Z., 2002, *ApJ*, 569, 558
 Ohsuga K., Mori M., Nakamoto T., Mineshige S., 2005, *ApJ*, 628, 368
 Omukai K., Schneider R., Haiman Z., 2008, *ApJ*, 686, 801
 Pacucci F., Ferrara A., 2015, *MNRAS*, 448, 104
 Pacucci F., Ferrara A., Grazian A., Fiore F., Giallongo E., Puccetti S., 2016, *MNRAS*, 459, 1432

- Pacucci F., Volonteri M., Ferrara A., 2015, MNRAS, 452, 1922
Paczynski B., Wiita P. J., 1980, A&A, 88, 23
Park K., Ricotti M., 2011, ApJ, 739, 2
Park K., Ricotti M., 2012, ApJ, 747, 9
Park K., Ricotti M., Natarajan P., Bogdanović T., Wise J. H., 2016, ApJ, 818, 184
Pezzulli E., Valiante R., Schneider R., 2016, MNRAS
Portegies Zwart S. F., Baumgardt H., Hut P., Makino J., McMillan S. L. W., 2004, Nature, 428, 724
Regan J. A., Johansson P. H., Wise J. H., 2014, ApJ, 795, 137
Sakurai Y., Vorobyov E. I., Hosokawa T., Yoshida N., Omukai K., Yorke H. W., 2016, MNRAS, 459, 1137
Sądowski A., Narayan R., 2016, MNRAS, 456, 3929
Sądowski A., Narayan R., McKinney J. C., Tchekhovskoy A., 2014, MNRAS, 439, 503
Schleicher D. R. G., Palla F., Ferrara A., Galli D., Latif M., 2013, A&A, 558, A59
Schneider R., Ferrara A., Natarajan P., Omukai K., 2002, ApJ, 571, 30
Shang C., Bryan G. L., Haiman Z., 2010, MNRAS, 402, 1249
Stone J. M., Norman M. L., 1992, ApJS, 80, 753
Stone N. C., Kuepper A. H. W., Ostriker J. P., 2016, arXiv:1606.01909
Tanaka T., Haiman Z., 2009, ApJ, 696, 1798
Tanaka T., Menou K., 2010, ApJ, 714, 404
Tanaka T. L., 2014, Classical and Quantum Gravity, 31, 244005
Venemans B. P. et al., 2013, ApJ, 779, 24
Visbal E., Haiman Z., Bryan G. L., 2014, MNRAS, 445, 1056
Volonteri M., 2010, A&A Rev., 18, 279
Volonteri M., Haardt F., Madau P., 2003, ApJ, 582, 559
Volonteri M., Rees M. J., 2005, ApJ, 633, 624
Volonteri M., Silk J., Dubus G., 2015, ApJ, 804, 148
Watarai K.-y., Fukue J., Takeuchi M., Mineshige S., 2000, PASJ, 52, 133
Whalen D., Norman M. L., 2006, ApJS, 162, 281
Willott C. J. et al., 2010, AJ, 139, 906
Wu X.-B. et al., 2015, Nature, 518, 512
Yajima H., Khochfar S., 2016, MNRAS, 457, 2423